15

Effects of Doping and Oxygen Nonstoichiometry on the Thermodynamic Properties of Some Multiferroic Ceramics

Speranta Tanasescu[1], Alina Botea[1]
and Adelina Ianculescu[2]
[1]*Department of Chemical Thermodynamics, Institute of Physical Chemistry Romanian Academy, Bucharest*
[2]*Polytechnics University of Bucharest, Bucharest Romania*

1. Introduction

In order to find new ways to tune, enhance and optimize the properties of novel materials designed for different applications, the thorough knowledge of their thermodynamics is essential. The determination of the thermodynamic data and the thermochemical investigation of the formation reactions are essential for evaluating the long term stability and compatibility when the compounds are used in different applications. A careful search for experimental values is very important so much the more the literature is rather scarce as concerns the quantitative thermodynamic data for many multicomponent systems exhibiting balances of competing interactions. The focus of our present work is on multiferroic ceramics, which represents a "complex materials" class presenting a combination of magnetic and electrical properties which make the studies of novel multifunctional structures a very important issue of research.

$BiFeO_3$ (BFO) of perovskite structure it is well known for its magnetic and ferroelectric ordering temperatures (T_N~640 K, T_C~1100 K) being one of the most attractive single phase multiferroic materials. For this reason there have been extensive studies of the structure, magnetic and electrical properties in bulk and in thin films, as well. Nevertheless, the wide potential for magnetoelectric applications of BFO may be inhibited because some major problems. Besides the small remanent polarization, the high coercive field and the inhomogeneous magnetic spin structure, the large leakage current it is still one of the major problems limiting device applications of BFO. The high conductivity and leakage found especially at higher temperatures were firstly considered caused by the high difficulty to produce single phase of $BiFeO_3$ (Catalan, 2009; Carvalho, 2008; Mitoseriu, 2005; Yuan, 2006). Very small impurities or parasitic phases segregated at grains at boundaries could have a doping effect and transform the dielectric into a semiconductor. Besides, as in most ferrites, the leakage current in $BiFeO_3$ could be attributed to the spontaneous change of the oxidation state of Fe (the partially reduction of Fe^{3+} ions to Fe^{2+}) causing a high number of oxygen vacancies as a result of electrical neutrality requirement, giving rise to thermal activated hoping conductivity and resulting in low

electrical resistivity (Palkar, 2002; Wang, 2004). Impurities and oxygen vacancies are also important for thin films, because they are known to artificially enhance the remanent magnetization (Catalan, 2009).

Forming binary solutions with other perovskites with good dielectric properties (like $BaTiO_3$, $PbTiO_3$ or $LnFeO_3$) was explored as a possible route for diminish the mentioned problems (Buscaglia, 2006; Ismailzade, 1981; Ianculescu, 2008; Kim, 2004, 2007; Kumar, 1999, 2000; Singh, 2008, 2009; Zhu 2004, Prihor Gheorghiu, 2010; Wang, 2005). The coexistence of ferroelectric and magnetic properties in $Bi_{1-x}Ba_xFe_{1-x}Ti_xO_3$ materials was noticed up to high temperatures (Kumar, 2000). However, in the $BiFeO_3$-rich region, these ceramics show weak magnetoelectric (ME) coupling effect, the problem of losses being only partially solved (Kumar, 1999).

The substitution of other elements for the Bi- and/or Fe-site was shown to enhance the ferroelectric and magnetic ordering in $BiFeO_3$. Doping with small amounts of rare earths proved to suppress the inhomogeneity of magnetic spin structure, stabilizing macroscopic magnetization of $BiFeO_3$ (Ivanova, 2003; Jiang, 2006; Sahu, 2007). Even though there are still questions about the structural evolution with composition (Catalan, 2009), previous studies on La-substituted $BiFeO_3$ indicate the decreasing of T_C and the increasing of T_N with La concentration (Chen, 2008; Sahu, 2007). On the other hand, substituting with Mn in $BiFeO_3$-based compounds was shown to improve the leakage current density and to induce changes in the magnetic order of the system, especially in the thin films (Azuma, 2007; Singh, 2007; Sahu, 2007; Habouti, 2007, Fukumura, 2009, Takahashi, 2007; Selbach, 2009, Wang, 2010). The simultaneous influence of La and Mn substitutions on the structural and functional properties of $BiFeO_3$ was discussed in a few papers (Bogatko, 1998; Ianculescu, 2009, Gagulin, 1997; Habouti, 2007; Kothari, 2007; Palkar, 2003; Pradhan, 2008; Zheng, 2010). Very little work was reported on the thermodynamic behaviour in the co-doped $(Bi,La)(Fe,Mn)O_3$ solid solutions (Gagulin, 1997; Tanasescu, 2010).

Recent investigations using advanced techniques, motivated by the prospect of new applications, have uncovered rich complexities that had not previously been recognized, when the development of new multifunctional bismuth ferrite perovskites, that combine sensitive responses to electric, magnetic, and stress fields, is intended [Ederer, 2005; Ramesh, 2007; Stroppa, 2010]. These phenomena occur at the crossover from localized to itinerant electronic behaviour and from ferroelectric (FE) to antiferromagnetic (AFE) displacive transitions, and are associated with dynamic, cooperative local deformations that are invisible to conventional diffraction studies. Due to the progress in methods for experimental analyzing distribution of elements at interfaces, some information has been accumulated on the chemical stabilities and properties of micro and nanostructured multifunctional materials. However the fundamental understanding was limited to rather simple cases. Such analyses need the thermodynamic data, because the driving forces for chemical reactions and diffusion can be given properly in terms of thermodynamic properties. This constitutes a considerable field of investigation, which is starting to be explored for both basic and applicative purposes (Boyd, 2011; Selbach, 2009; Tanasescu, 2004, 2008).

The present studies are focused upon the investigation of the effect of different compositional variables on the thermochemical properties and thermodynamic stability of multiferroic ceramics. Some compounds from specific systems were selected for discussion: multiferroic lead-free ceramics based on the $(1-x)BiFeO_3$ - $xBaTiO_3$ ($0 \le x \le 0.30$) solid solutions and $Bi_{1-x}La_xFe_{1-y}Mn_yO_3$ with x = 0.1; y = 0 - 0.5 perovskite-type materials.

2. Experimental

2.1 Sample preparation

(1-x)$BiFeO_3$ – x$BaTiO_3$ ($0 \le x \le 0.30$) ceramic samples were prepared by classical solid state reaction method from high purity oxides and carbonates: Bi_2O_3 (Fluka), Fe_2O_3 (Riedel de Haen), TiO_2 (Merck) and $BaCO_3$ (Fluka), by a wet homogenization technique in isopropyl alcohol. The place of the selected compositions on the $BiFeO_3$ – $BaTiO_3$ tie line of the quaternary Bi_2O_3 – BaO – Fe_2O_3 –TiO_2 system is also presented in Fig. 1(a).

The mixtures were granulated using a 4 % PVA (polyvinyl alcohol) solution as binder agent, shaped by uniaxial pressing at 160 MPa into pellets of 20 mm diameter and ~3 mm thickness. The presintering thermal treatment was carried out in air, at 923 K, with 2 hours plateau. The samples were slowly cooled, then ground, pressed again into pellets of 10 mm diameter and 1- 2 mm thickness and sintered in air, with a heating rate of 278 K/min, for 1 hour at 973 and 1073 K, respectively (Ianculescu, 2000; Prihor, 2009; Prihor Gheorghiu, 2010).

$Bi_{0.9}La_{0.1}Fe_{1-x}Mn_xO_3$ ($0 \le x \le 0.5$) ceramics have been prepared by the same route, in the same conditions and starting from the same raw materials (Ianculescu, 2009). The place of the investigated compositions in the quaternary Bi_2O_3 – La_2O_3 – Fe_2O_3 – Mn_2O_3 system is presented in Fig. 1(b).

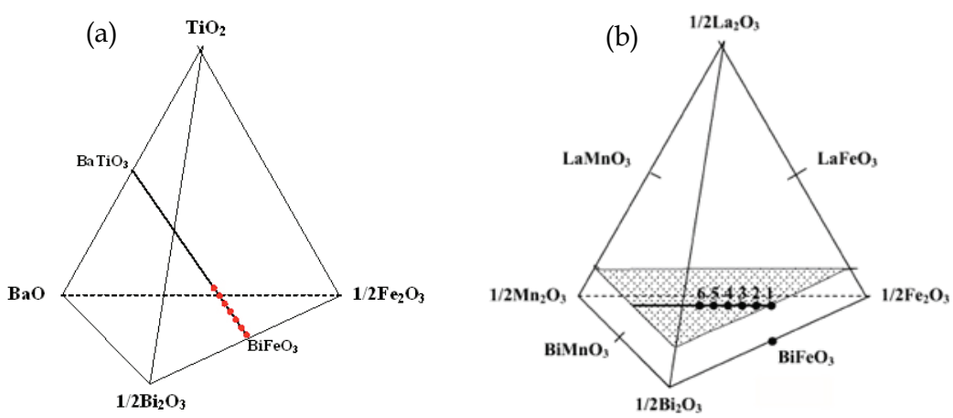

Fig. 1. Place of the investigated compositions: (a) $Bi_{1-x}Ba_xFe_{1-x}Ti_xO_3$ in the quaternary Bi_2O_3 – BaO – Fe_2O_3 –TiO_2 system; (b) $Bi_{0.9}La_{0.1}Fe_{1-x}Mn_xO_3$ in the quaternary Bi_2O_3 – La_2O_3 – Fe_2O_3 – Mn_2O_3 system

2.2 Sample characterization

In both $Bi_{1-x}Ba_xFe_{1-x}Ti_xO_3$ and $Bi_{0.9}La_{0.1}Fe_{1-x}Mn_xO_3$ systems, the phase composition and crystal structure of the ceramics resulted after sintering were checked with a SHIMADZU XRD 6000 diffractometer with Ni-filtered CuKα radiation (λ = 1.5418 Å), 273.02 K scan step and 1 s/step counting time. To estimate the structural characteristics (unit cell parameter and rhombohedral angle) the same step increment but with a counting time of 10 s/step, for 2θ ranged between 293–393 K was used. Parameters to define the position, magnitude and shape of the individual peaks are obtained using the pattern fitting and profile analysis of the original X-ray 5.0 program. The lattice constants calculation is based on the Least Squares Procedure (LSP) using the linear multiple regressions for several XRD lines, depending on the unit cell symmetry.

A HITACHI S2600N scanning electron microscope SEM coupled with EDX was used to analyze the ceramics microstructure.

The solid-oxide electrolyte galvanic cells method was employed to obtain the thermodynamic properties of the samples. As shown in previous papers (Tanasescu, 1998, 2003, 2009) the thermodynamic stability limits of the $ABO_{3-\delta}$ perovskite-type oxides are conveniently situated within the range of oxygen chemical potentials that can be measured using galvanic cells containing 12.84 wt.% yttria stabilized zirconia solid electrolyte and an iron-wüstite reference electrode. The design of the apparatus, as well as the theoretical and experimental considerations related to the applied method, was previously described (Tanasescu, 1998, 2011).

The measurements were performed in two principal different ways:

- Under the open circuit conditions, keeping constant all the intensive parameters, when the electromotive force (EMF) measurements give information about the change in the Gibbs free energy for the virtual cell reaction. The EMF measurements were performed in vacuum at a residual gas pressure of 10^{-7} atm. The free energy change of the cell is given by the expression:

$$\Delta G_{\text{cell}} = \mu_{O_2} - \mu_{O_{2(\text{ref})}} = 4FE \tag{1}$$

where E is the steady state EMF of the cell in volts; μ_{O_2} , $\mu_{O_{2(\text{ref})}}$ are respectively, the oxygen chemical potentials of the sample and the reference electrode and F is the Faraday constant (F=96.508 kJ/V equiv.).

By using the experimental values of the electromotive force of the cell and knowing the free energy change of the reference electrode (Charette, 1968; Kelley 1960, 1961), the values of the relative partial molar free energy of the solution of oxygen in the perovskite phase and hence the pressures of oxygen in equilibrium with the solid can be calculated:

$$\Delta\overline{G}_{O_2} = RT \ln p_{O_2} \tag{2}$$

The relative partial molar enthalpies and entropies were obtained according to the known relationships (Tanasescu, 1998, 2011):

$$\frac{\partial \dfrac{\Delta\overline{G}_{O_2}}{T}}{\partial T} = -\frac{\Delta\overline{H}_{O_2}}{T^2} \tag{3}$$

$$\Delta\overline{G}_{O_2} = \Delta\overline{H}_{O_2} - T\Delta\overline{S}_{O_2} \tag{4}$$

The overall uncertainty due to the temperature and potential measurement (taking into account the overall uncertainty of a single measurement and also the quoted accuracy of the voltmeter) was ±1.5 mV. This was equivalent to ±0.579 kJ mol^{-1} for the free energy change of the cell. Considering the uncertainty of ±0.523 kJ mol^{-1} in the thermodynamic data for the iron-wüstite reference (Charette, 1968; Kelley 1960, 1961), the overall data accuracy was estimated to be ±1.6 kJ mol^{-1}. For the enthalpies the errors were ±0.45 kJ mol^{-1} and for the entropies ±1.1 J mol^{-1} K^{-1}. Errors due to the data taken from the literature are not included in these values because of the unavailability of reliable standard deviations.

- By using a coulometric titration technique coupled with EMF measurements (Tanasescu, 2011), method which proved to be especially useful in the study of the compounds with properties highly sensitive to deviations from stoichiometry. The obtained results allow us to evidence the influence of the oxygen stoichiometry change on the thermodynamic properties. The titrations were performed *in situ* at 1073 K by using a Bi-PAD Tacussel Potentiostat. A constant current (I) is passed through the cell for a predetermined time (t). Because the transference number of the oxygen ions in the electrolyte is unity, the time integral of the current is a precise measure of the change in the oxygen content (Tanasescu, 1998; 2011). According to Faraday's law, the mass change $|\Delta m|$ (g) of the sample is related to the transferred charge Q (A·sec) by:

$$|\Delta m| = 8.291 \cdot 10^{-5} Q \tag{5}$$

As one can see, a charge of $1 \cdot 10^{-5}$ A sec, which is easily measurable corresponds to a weight change of only $8x\ 10^{-10}$ g. This makes it possible to achieve extremely high compositional resolution, and very small stoichiometric widths in both deficient and excess oxygen domains can be investigated. Thus, the effect of the oxygen stoichiometry can be correlated with the influence of the A- and B-site dopants.
After the desired amount of electricity was passed through the cell, the current circuit was opened, every time waiting till the equilibrium values were recorded (about three hours). Practically, we considered that EMF had reached its equilibrium value when three subsequent readings at 30 min intervals varied by less than 0.5 mV. After the sample reached equilibrium, for every newly obtained composition, the temperature was changed under open-circuit condition, and the equilibrium EMFs for different temperatures between 1073 and 1273 K were recorded.
Differential scanning calorimetric measurements were performed with a *SETSYS Evolution Setaram* differential scanning calorimeter (Marinescu, in press; Tanasescu, 2009). For data processing and analyses the Calisto–AKTS software was used. The DSC experiments were done on ceramic samples under the powder form, at a heating rate 10°C/min. and by using Ar with purity > 99.995% as carrier gas. For measurements and corrections identical conditions were set (Marinescu, in press). The critical temperatures corresponding to the ferro-para phase transitions, the corresponding enthalpies of transformations as well as heat capacities were obtained according to the procedure previously described (Marinescu, in press; Tanasescu, 2009).

3. Results and discussion

3.1 $BiFeO_3$-$BaTiO_3$ system

3.1.1 Phase composition and crystalline structure

The room temperature XRD patterns (Fig. 2(a)) show perovskite single-phase, in the limit of XRD accuracy for all the investigated compositions after pre-sintering at 923 K/2 h followed by sintering at 1073 K/1 h and slow cooling. For all investigated ceramics, perovskite structure of rhombohedral R3c symmetry was identified, with a gradual attenuation of the rhombohedral distortion with the increase of $BaTiO_3$ content. This tendency to a gradual change towards a cubic symmetry with the $BaTiO_3$ addition is proved by the cancellation of the splitting of the XRD (110), (111), (120), (121), (220), (030) maxima specific to pure $BiFeO_3$ ($2\theta \approx 31.5^o$, 39^o, 51^o, 57^o, 66^o, 70^o, 75^o), as observed in the detailed representation from Fig.

2(b). The evolution of the structural parameters provides an additional evidence for the influence of $BaTiO_3$ admixture in suppressing rhombohedral distortion (Fig. 3). Besides, the expansion of the lattice parameters induced by an increasing barium titanate content in $(1-x)BiFeO_3 - xBaTiO_3$ system was also pointed out (Prihor, 2009).

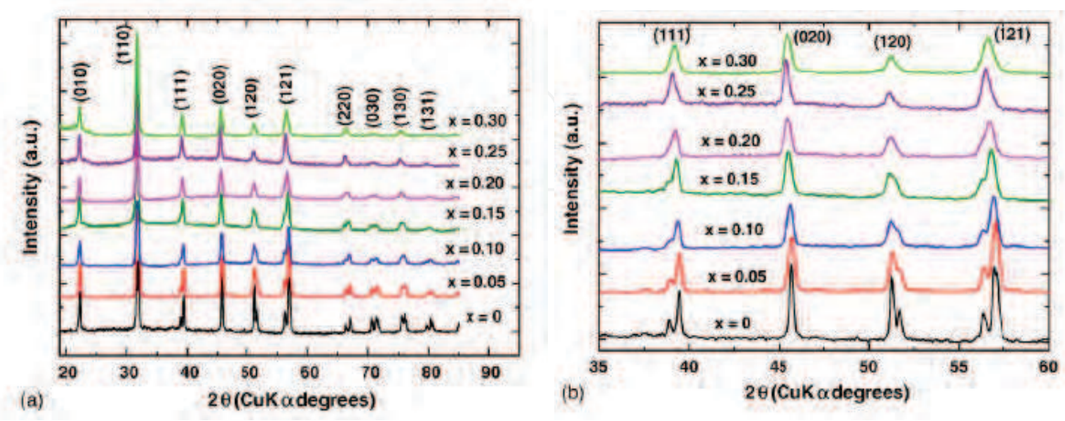

Fig. 2. (a) Room temperature X-ray diffraction patterns of the $(1-x)BiFeO_3 - xBaTiO_3$ ceramics pre-sintered at 923 K/2 h, sintered at 1073 K/1 h and slow cooled; (b) detailed XRD pattern showing the cancellation of splitting for (1 1 1), (1 2 0) and (1 2 1) peaks, when increasing x.

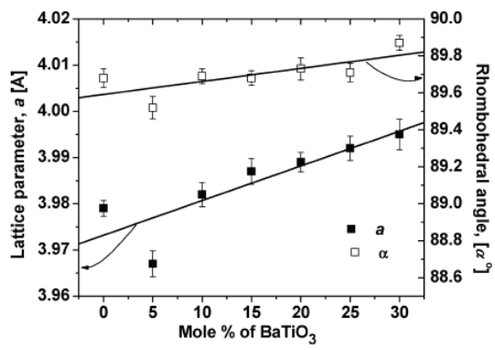

Fig. 3. Evolution of the structural parameters versus $BaTiO_3$ content.

3.1.2 Microstructure

Surface SEM investigations were performed on both presintered and sintered samples. The SEM image of $BiFeO_3$ ceramic obtained after presintering at 923 K shows that the microstructure consists of intergranular pores and of grains of various size (the average grain size was estimated to be ~ 20 μm), with not well defined grain boundaries, indicating an incipient sintering stage (Fig. 4(a)). The SEM images of samples with x = 0.15 and x = 0.30 (Figs. 4(b) and 4(c)) indicate that barium titanate addition influences drastically the microstructure. Thus, one can observe that $BaTiO_3$ used as additive has an inhibiting effect on the grain growth process and, consequently, a relative homogeneous microstructure, with a higher amount of intergranular porosity and grains of ~ one order of magnitude smaller than those ones of non-modified sample, were formed in both cases analyzed here.

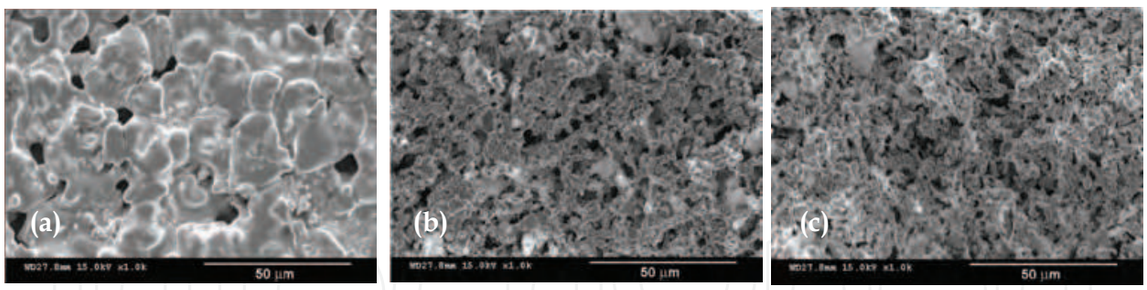

Fig. 4. Surface SEM images of (1-x)$BiFeO_3$ – x$BaTiO_3$ ceramics obtained after presintering at 923 K/2 hours: (a) x = 0, (b) x = 0.15 and (c) x = 0.30

$BiFeO_3$ pellet sintered at 1073 K/1h exhibits a heterogeneous microstructure with bimodal grain size distribution, consisting from large grains with equivalent average size of ~ 25 μm and small grains of 3 - 4 μm (Fig. 5(a)). The micrograph of the ceramic sample with x = 0.15 (Fig. 5(b)) shows that the dramatic influence of the $BaTiO_3$ on the microstructural features is maintained also after sintering. Thus, a significant grain size decrease was observed for sample with x = 0.15. Further increase of $BaTiO_3$ content to x = 0.30 (Fig. 5(c)) seems not to determine a further drop in the average grain size. Consequently, in both cases a rather monomodal grain size distribution and relative homogenous microstructures, consisting of finer (submicron) grains were observed (Ianculescu, 2008; Prihor, 2009). Irrespective of $BaTiO_3$ content, the amount of intergranular porosity is significantly reduced in comparison with the samples resulted after only one-step thermal treatment. This indicates that sintering strongly contributes to densification of the $Bi_{1-x}Ba_xFe_{1-x}Ti_xO_3$ ceramics.

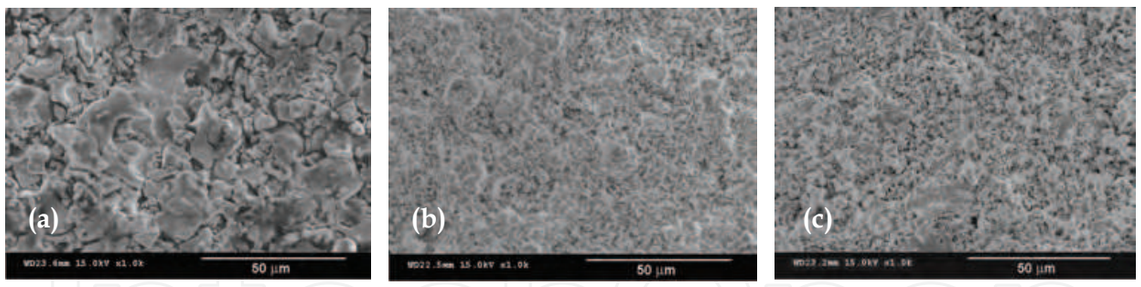

Fig. 5. Surface SEM images of (1-x)$BiFeO_3$ – x$BaTiO_3$ ceramics obtained after presintering at 923 K/2 hours and sintering at 1073 K/1 hour: (a) x = 0, (b) x = 0.15 and (c) x = 0.30

3.1.3 Thermodynamic properties of $Bi_{1-x}Ba_xFe_{1-x}Ti_xO_3$

Of particular interest for us is to evidence how the appropriate substitutions could influence the stability of the $Bi_{1-x}Ba_xFe_{1-x}Ti_xO_3$ perovskite phases and then to correlate this effect with the charge compensation mechanism and the change in the oxygen nonstoichiometry of the samples.

In a previous work (Tanasescu, 2009), differential scanning calorimetric experiments were performed in the temperature range of 773-1173 K in order to evidence the ferro-para phase transitions by a non-electrical method. Particular attention is devoted to the high temperature thermodynamic data of these compounds for which the literature is rather scarce. Both the temperature and composition dependences of the specific heat capacity of

the samples were determined and the variation of the Curie temperature with the composition was investigated. The effect of the BaTiO3 addition to BiFeO3 was seen as the decrease of the Curie transition temperature and of the corresponding enthalpy of transformation and heat capacity values (Tanasescu, 2009) (Fig. 6). A sharp decline in the T_C was pointed out for $BiFeO_3$ rich compositions (Fig. 6). In fact, the *C*p of the rhombohedral phase (x = 0) is obviously larger than that of the $Bi_{1-x}Ba_xFe_{1-x}Ti_xO_3$ perovskite phases, whereas the *C*p of each phase shows a weak composition dependence below the peak temperature. In particular, the value of *C*p for x = 0.3 was found to be fairly low, which we did not show in the figure. The decreasing of the ferroelectric – paraelectric transition temperature with the increase of the $BaTiO_3$ amount in the composition of the solid solutions with x = 0 ÷ 0.15 indicated by the DSC measurements is in agreement with the dielectric data reported by Buscaglia et al (Buscaglia, 2006).

Some reasons for this behaviour could be taken into account. First of all, these results confirm our observations that the solid solution system $BiFeO_3$ – $BaTiO_3$ undergoes structural transformations with increasing content of $BaTiO_3$. The decrease of the ferroelectric-paraelectric transition temperature *T*c observed for the solid solution (1-*x*)$BiFeO_3$ – *x*$BaTiO_3$ may be ascribed to the decrease in unit cell volume caused by the $BaTiO_3$ addition. Addition of Ba^{2+} having empty p orbitals, reduces polarization of core electrons and also the structural distorsion. The low value obtained for *C*p at x = 0.3 is in accordance with the previous result indicating that ferroelectricity disappears in samples above x ~ 0.3 (Kumar, 2000).

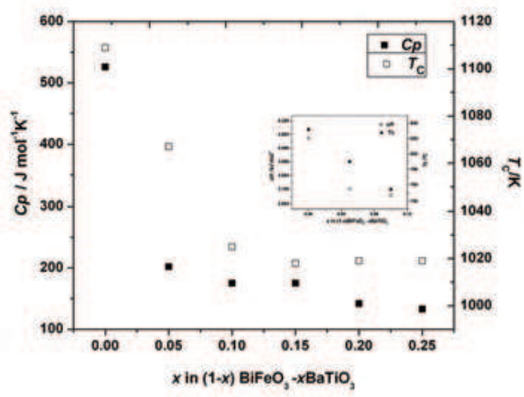

Fig. 6. Variation of the Curie transition temperature T_C and of the heat capacity *C*p with composition. Inset: Variation of T_C and enthalpy of transformation for $BiFeO_3$ rich compositions (x=0; 0.05; 0.1) (Tanasescu, 2009)

At the same time, the diffused phase transitions for compositions with x > 0.15 could be explained in terms of a large number of A and B sites occupied by two different, randomly distributed cationic specimens in the perovskite ABO_3 lattice. Previous reports on the substituted lanthanum manganites indicate that the mismatch at the A site creates strain on grain boundaries which affect the physical properties of an ABO_3 perovskite (Maignan, 2000). Besides, the role of charge ordering in explaining the magnetotransport properties of the variable valence transition metals perovskite was emphasized (Jonker, 1953). Investigating the influence of the dopants and of the oxygen nonstoichiometry on spin dynamics and thermodynamic properties of the magnetoresistive perovskites, Tanasescu et

al (Tanasescu, 2008, 2009) pointed out that the remarkable behaviour of the substituted samples could be explained not only qualitatively by the structural changes upon doping, but also by the fact that the magneto-transport properties are extremely sensitive to the chemical defects in oxygen sites.

Though the effects of significant changes in the overall concentration of defects is not fully known in the present system of materials, extension of the results obtained on substituted manganites, may give some way for the correlation of the electrical, magnetic and thermodynamic properties with the defect structure. The partial replacement of Bi^{3+} with Ba^{2+} cations acting as acceptor centers could generate supplementary oxygen vacancies as compensating defects, whereas the Ti^{4+} solute on Fe^{3+} sites could induce cationic vacancies or polaronic defects by $Fe^{3+} \rightarrow Fe^{2+}$ transitions. The presence of the defects and the change of the Fe^{2+}/ Fe^{3+} ratio is in turn a function not only of the composition but equally importantly of the thermal history of the phase. Consequently, an understanding of the high temperature defect chemistry of phases is vital, if an understanding of the low temperature electronic and magnetic properties is to be achieved. To further evaluate these considerations, and in order to discriminate against the above contributions, experimental insight into the effects of defect types and concentrations on phase transitions and thermodynamic data could give a valuable help.

For discussion was chosen the compound $Bi_{0.90}Ba_{0.10}Fe_{0.90}Ti_{0.10}O_3$ for which strong magnetoelectric coupling of intrinsic multiferroic origin was reported (Singh, 2008). The results obtained in the present study by using EMF and solid state state coulometric titration techniques are shown in the following.

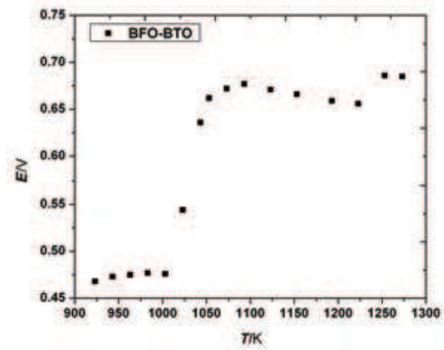

Fig. 7. Temperature dependence of EMF for $Bi_{0.90}Ba_{0.10}Fe_{0.90}Ti_{0.10}O_3$

The recorded EMF values obtained under the open circuit condition in the temperature range 923-1273 K are presented in Fig. 7. The thermodynamic data represented by the relative partial molar free energies, enthalpies and entropies of the oxygen dissolution in the perovskite phase, as well as the equilibrium partial pressures of oxygen have been calculated and the results are depicted in Figs. 8-11. A complex behavior which is dependent on the temperature range it was noticed, suggesting a change of the predominant defects concentration for the substituted compound.

As one can see in Fig. 7, at low temperatures, between 923 and ~1000 K, EMF has practically the same value E=0.475 V. Then, Fig. 7 distinctly shows a break in the EMF vs. temperature relation at about 1003 K, indicating a sudden change in the thermodynamic parameters. A strong increase of the partial molar free energy and of the partial pressure of oxygen was

observed until 1050 K (Figs. 8 and 9) which can be due to structural transformation related to the charge compensation of the material system. Then, on a temperature interval of about 40 K the increasing of the energies values is smaller. After ~ 1090 K a new change of the slope in the $\Delta\overline{G}_{O_2}$ and $\log p_{O_2}$ variation is registered on a temperature interval of about 130 degrees, followed again, after 1223 K, by a sudden change of the thermodynamic data, the higher $\Delta\overline{G}_{O_2}$ value being obtained at about 1260 K.

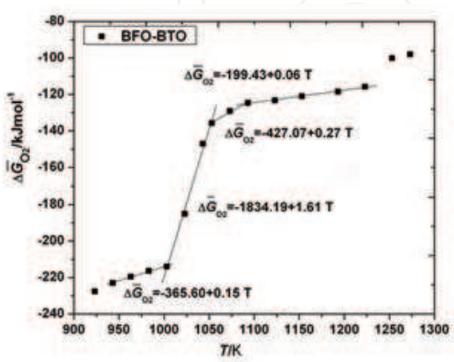

Fig. 8. Variation of $\Delta\overline{G}_{O_2}$ with temperature - linear fit in the selected temperature ranges: 943-1003 K, 1003-1053 K, 1053-1093 K and 1093-1223 K

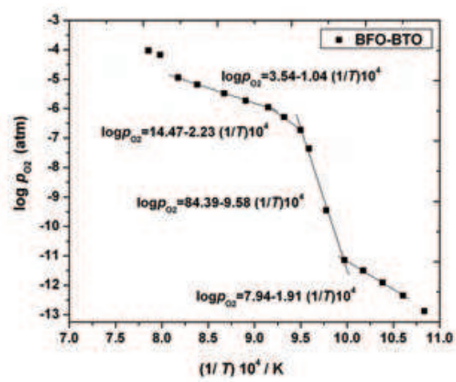

Fig. 9. The plot of $\log p_{O_2}$ vs. $1/T$ for the selected temperatures ranges

The break point at about 1003 K is mainly due to first order phase transition in $Bi_{0.90}Ba_{0.10}Fe_{0.90}Ti_{0.10}O_3$ associated with the ferroelectric to the paraelectric transition T_C. The 10% $BaTiO_3$ substitution reduces the ferroelectric transition temperature of $BiFeO_3$ with about 100K. This transition is also evident from calorimetric measurements (Tanasescu, 2009). The less abrupt first order transition at 1050 K is qualitatively in concordance with the transition to the γ polymorph which was previously identified in the literature for $BiFeO_3$ at 1198-1203K (Arnold, 2010; Palai, 2008; Selbach, 2009).

In Fig. 10 we represented the partial molar free energies of oxygen dissolution obtained in this study for both $Bi_{0.90}Ba_{0.10}Fe_{0.90}Ti_{0.10}O_3$ and $BiFeO_3$ at temperatures lower than their specific ferroelectric transition temperatures. We would like to specify that in the case of $BiFeO_3$, the EMF measurements were performed at temperatures not higher than 1073 K due

to the instability of $BiFeO_3$ at higher temperatures. As one can see in Fig. 10, at 923 K, the partial molar free energies of oxygen dissolution in $BiFeO_3$ and $Bi_{0.90}Ba_{0.10}Fe_{0.90}Ti_{0.10}O_3$ samples are near each other. With increasing temperature, the highest $\Delta\overline{G}_{O_2}$ values were obtained for $BiFeO_3$, suggesting an increased oxygen vacancies concentration in this compound. The result could be explained by the fact that at low temperatures the conduction is purely intrinsic and the anionic vacancies created are masked by impurity conduction. As the temperature increases, conduction becomes more extrinsic (Warren, 1996), and conduction due to the oxygen vacancies surface. This fact is also evident from the density measurements (Kumar, 2000), as well as electron paramagnetic resonance studies on perovskites (Warren, 2006). The increased concentration of oxygen vacancies in $BiFeO_3$ is consistent with the large leakage current reported for $BiFeO_3$ (Gu, 2010; Qi, 2005; Palkar, 2002; Wang, 2004). The electrical characteristics (Qi, 2005) indicated that the main conduction mechanism for pure BFO was space charge limited, and associated with free carriers trapped by oxygen vacancies. The coexistence of Fe^{3+} and Fe^{2+} causes electron hopping between Fe^{3+} and Fe^{2+} ions, oxygen vacancies acting as a bridge between them, which increases the leakage current. According to the defect chemistry theory, doping $BiFeO_3$ with aliovalent ions should change the oxidation state of iron and the concentration of oxygen vacancies. Qi and coworkers (Qi, 2005) have suggested as possible mechanisms to achieve the charge compensation in the 4+ cation-doped material: filling of oxygen vacancies, decrease of cation valence by formation of Fe^{2+}, and creation of cation vacancies. Based on our results, the doping with Ti^{4+} is expected to eliminate oxygen vacancies causing the decreasing of $\Delta\overline{G}_{O_2}$ and $\log p_{O_2}$ values.

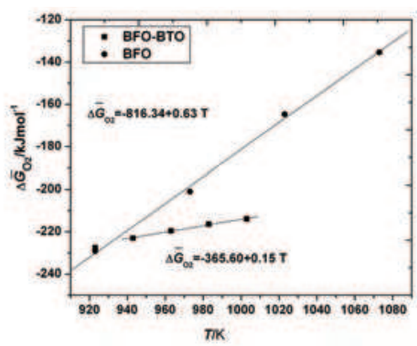

Fig. 10. Variation of $\Delta\overline{G}_{O_2}$ with temperature - linear fit in the temperature range 943-1003 K for $Bi_{0.90}Ba_{0.10}Fe_{0.90}Ti_{0.10}O_3$ (BFO-BTO) and 923-1073 K for $BiFeO_3$ (BFO)

Further clarification could be achieved by determining $\Delta\overline{H}_{O_2}$ and $\Delta\overline{S}_{O_2}$ values in particular temperature ranges in which the partial molar free energies are linear functions of temperature. Comparing the values obtained for $Bi_{0.90}Ba_{0.10}Fe_{0.90}Ti_{0.10}O_3$ in the temperature interval of 943-1003 K with the corresponding enthalpies and entropies values of $BiFeO_3$ in the 923-1073 K range (Fig. 11) one can observe that for the substituted compound, $\Delta\overline{H}_{O_2}$ and $\Delta\overline{S}_{O_2}$ values strongly increase (with ~450 kJ mol^{-1} and ~480 J mol^{-1} K^{-1} respectively). This finding can be explained by the relative redox stability of the B-site ions which seems to modify both the mobility and the concentration of the oxygen vacancies. It is interesting to note that increasing temperature, after the first transition point, the enthalpies and entropies values strongly decrease (with ~ 468 kJ mol^{-1} and ~1.4 kJ mol^{-1} K^{-1} respectively) up to more

negative values. The negative values obtained for the relative partial entropies of oxygen dissolution at high temperature are indicative for a metal vacancy mechanism. Above 1053 K both the enthalpy and entropy increase again with increasing the temperature. The thermal reduction for transition metals tends to be easier with Ba doping. These may explain the reason for the different behaviors at higher temperature zone. Besides, oxygen vacancy order also show contribution to the observed phenomena, the increasing of the enthalpy and entropy values being an indication that the oxygen vacancies distribute randomly on the oxygen sublattice.

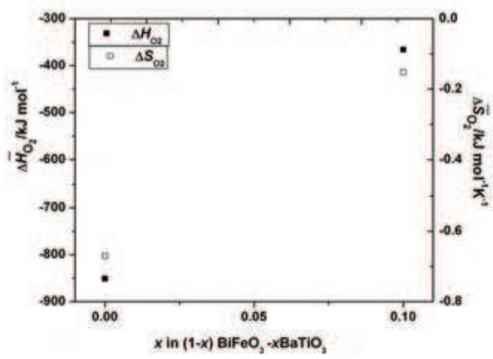

Fig. 11. $\Delta\overline{H}_{O_2}$ and $\Delta\overline{S}_{O_2}$ as a function of $BaTiO_3$ content (x) at temperatures lower than ferroelectric transition temperatures.

In order to further evaluate the previous results, the influence of the oxygen stoichiometry change on the thermodynamic properties has to be examined. The variation of the thermodynamic data of oxygen deficient $Bi_{0.90}Ba_{0.10}Fe_{0.90}Ti_{0.10}O_{3-\delta}$ samples was analyzed at the relative stoichiometry change $\Delta\delta$ = 0.01. In Figures 12 (a) and (b), two sets of data obtained before and after the isothermal titration experiments are plotted. Higher $\Delta\overline{G}_{O_2}$ and $\log p_{O_2}$ values are obtained after titration at all temperatures until 1223 K; above 1223 K, the values after titration are lower than the corresponding values before titration.

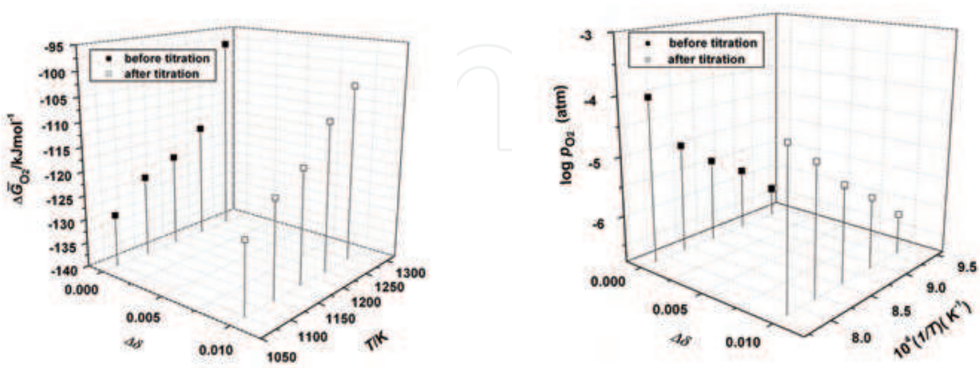

(a) (b)

Fig. 12. Variation of (a) $\Delta\overline{G}_{O_2}$ and (b) $\log p_{O_2}$ with temperature and oxygen stoichiometry change for $Bi_{0.90}Ba_{0.10}Fe_{0.90}Ti_{0.10}O_3$

Regarding the changes of $\Delta\overline{H}_{O_2}$ and $\Delta\overline{S}_{O_2}$ corresponding to the temperature range of 1093-1223 K (Fig. 13), one can observe that for $Bi_{0.90}Ba_{0.10}Fe_{0.90}Ti_{0.10}O_3$, both the variations of enthalpy and entropy decrease with the stoichiometry change suggesting the increase in the binding energy of oxygen and the change of order in the oxygen sublattice of the perovskite-type structure. The values of the relative partial entropies of oxygen dissolution are negative and this is indicative for a metal vacancy mechanism (Töfield, 1974). Due to the large decrease in $\Delta\overline{S}_{O_2}$, it is considered that the oxygen vacancies would not randomly distribute on all of the oxygen sites but they would be distributed to some particular oxygen sites. It is also possible that the vacancy distribution is related to some crystallographic distortions or ordering of metal sites.

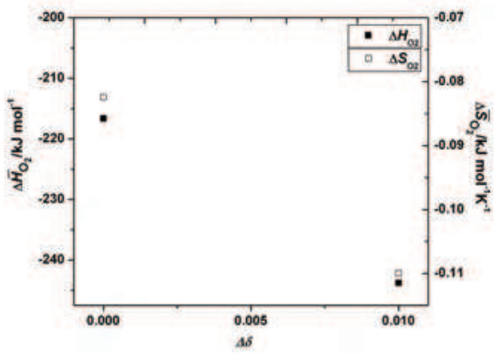

Fig. 13. $\Delta\overline{H}_{O_2}$ and $\Delta\overline{S}_{O_2}$ as a function of the oxygen stoichiometry change ($\Delta\delta = 0.01$)

Presently, however, further details and measurements of the energy and entropy of oxygen incorporation into $BiFeO_3$-based materials at different values of nonstoichiometry δ are necessary in order to make clear the vacancy distribution with the stoiochiometry change.

3.2 $Bi_{1-x}La_xFe_{1-y}Mn_yO_3$ (x=0.1; y=0-0.5)

3.2.1 Phase composition and crystalline structure

The room temperature X-ray diffraction pattern obtained for the presintered sample corresponding to the mixture 1 ($Bi_{0.9}La_{0.1}FeO_3$) shows a single phase composition, consisting of the well-crystallized perovskite phase (Fig. 14(a)). A small Mn addition ($x \leq 0.1$) does not change the phase composition. The increase of the manganese amount to x = 0.2 determines the segregation of a small amount of $Bi_{36}Fe_2O_{57}$ secondary phase identified at the detection limit. For $x \geq 0.4$ also small quantities of $Bi_2Fe_4O_9$ was detected as secondary phase, indicating the beginning of a decomposition process (Fig 14(a)).

From the structural point of view the XRD data pointed out that all the samples exhibit hexagonal *R*3c symmetry, similar to the structure of the paternal non-modified $BiFeO_3$ compound. Similar to $Bi_{1-x}Ba_xFe_{1-x}Ti_xO_3$ solid solutions, the increase of the manganese content does not determine the change of spatial group. However, certain distortions clearly emphasized by the cancellation of the splitting of some characteristic XRD peaks take place. Thus, Fig. 14(b) shows the evolution of the profile and position of the neighbouring (006) and (202) peaks specific to the $Bi_{0.9}La_{0.1}O_3$ composition when Mn is added in the system. One can observe that an amount of only 10% Mn replacing Fe^{3+} in the perovskite structure is enough to eliminate the (006) peak in the characteristic XRD pattern. A shift of the position

of the main diffraction peaks toward higher 2θ values was also pointed out (for exampe the (002) peak shifts from 2θ = 39.5° for $Bi_{0.9}La_{0.1}FeO_3$ to 2θ = 39.82° for $Bi_{0.9}La_{0.1}Fe_{0.5}Mn_{0.5}O_3$). The increase of the manganese concentration determines the decrease of both *a* and *c* lattice parameters (Fig. 15(a)) and therefore a gradual contraction of the unit cell volume (Fig. 15(b)). This evolution suggests that most of the manganese ions are more probably incorporated on the *B* site of the perovskite network as Mn^{4+}, causing the decrease of the network parameters because of the smaller ionic radius of Mn^{4+} (0.60 Å), comparing with that one corresponding to Fe^{3+} (0.64 Å). These results are in agreement with those ones reported by Palkar et al (Palkar, 2003).

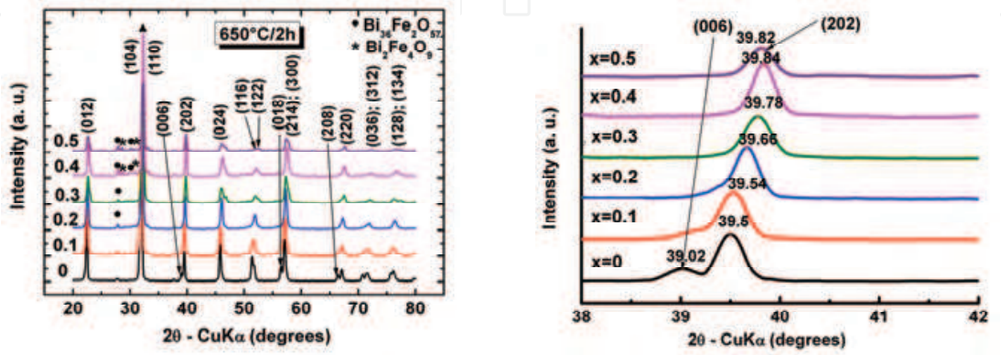

(a) (b)

Fig. 14. (a) Room temperature X-ray diffraction patterns for $Bi_{0.9}La_{0.1}Fe_{1-x}Mn_xO_3$ ceramics thermally treated at 923 K for 2 hours; (b) detailed XRD pattern showing the disappearance of (0 0 6) peak

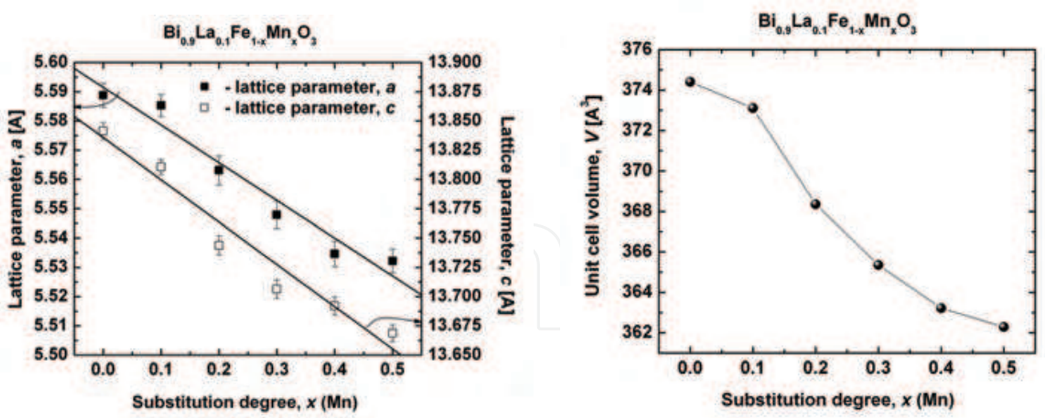

(a) (b)

Fig. 15. Evolution of the structural parameters versus Mn content for the $Bi_{0.9}La_{0.1}Fe_{1-x}Mn_xO_3$ ceramics sintered at 1073 K for 1 hour: (a) lattice parameters and (b) unit cell volume

3.2.2 Microstructure

As for $Bi_{1-x}Ba_xFe_{1-x}Ti_xO_3$ ceramics, SEM analyses were performed firstly on the pellets surface thermally treated at 923 K/2h. The surface SEM image of the $Bi_{0.9}La_{0.1}FeO_3$ sample

indicates the obtaining of a non-uniform and porous microstructure, consisting from grains of variable sizes and a significant amount of intergranular porosity (fig. 16(a)). For the sample with x = 0.20, the presence of the manganese in the system induces the inhibition of the grain growth process and has a favourable effect on the densification (Fig. 16(b)).

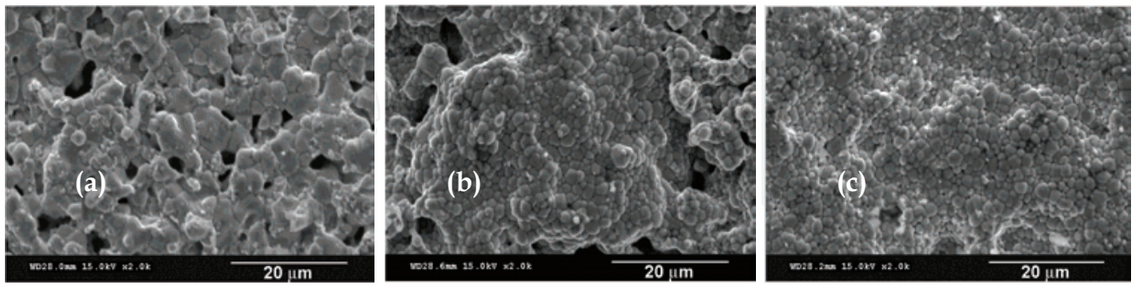

Fig. 16. Surface SEM images of: (a) $Bi_{0.9}La_{0.1}FeO_3$; (b) $Bi_{0.9}La_{0.1}Fe_{0.8}Mn_{0.2}O_3$ and (c) $Bi_{0.9}La_{0.1}Fe_{0.5}Mn_{0.5}O_3$ presintered at 925 K for 2 hours

The further increase of the Mn content to x = 0.50 enhances the densification, but seems to have not anymore a significant influence on the average grain size. Thus, the $Bi_{0.9}La_{0.1}Fe_{0.5}Mn_{0.5}O_3$ ceramic shows a dense, fine-grained (average grain size of ~ 2 μm) and homogeneous microstructure with a monomodal grain size distribution (Fig. 16(c)).
The same trend of the decrease of the average grain size with the addition of both La and Mn solutes was also observed in the case of the ceramics sintered at 1073 K for 1 hour. Thereby, unlike the non-homogeneous, rather coarse-grained $BiFeO_3$ sample (Fig. 5(a)), the average grain size in the La-modified $Bi_{0.9}La_{0.1}FeO_3$ ceramic is of only ~ 4 μm (Fig. 17(a)). The increase of Mn addition causes a further decrease of the average grain size to ~ 2 μm and a tendency to coalescence of the small grains in larger, well-sintered blocks (Fig. 17(b) and 17(c)).

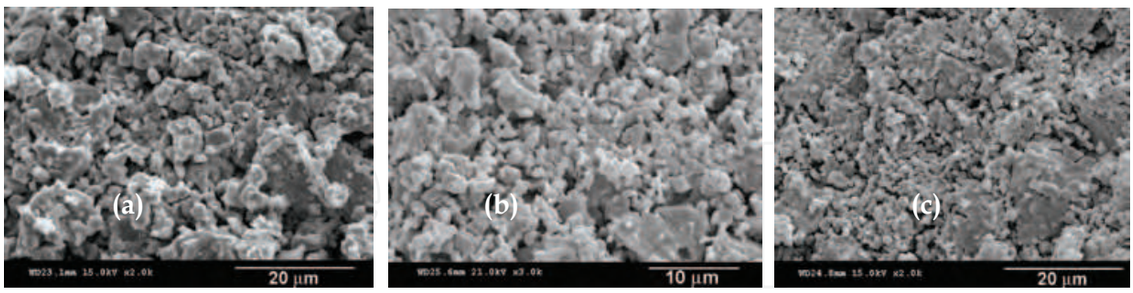

Fig. 17. Surface SEM images of: (a) $Bi_{0.9}La_{0.1}FeO_3$; (b) $Bi_{0.9}La_{0.1}Fe_{0.8}Mn_{0.2}O_3$ and (c)$Bi_{0.9}La_{0.1}Fe_{0.5}Mn_{0.5}O_3$ ceramics sintered at 1073 K for 1 hour.

3.3.3 Thermodynamic properties of $Bi_{1-x}La_xFe_{1-y}Mn_yO_3$ (x=0.1; y=0.2; 0.3)

Emphasizing the role of charge ordering in explaining the magnetotransport properties of the manganites, Jonker and van Santen considered that the local charge in the doped manganites is balanced by the conversion of Mn valence between Mn^{3+} and Mn^{4+} and the creation of oxygen vacancies, as well (Jonker, 1953). Investigating the influence of the dopants and of the nonstoichiometry on spin dynamics and thermodynamic properties of

the magnetoresistive perovskites, Tanasescu et al (Tanasescu, 2008, 2009) demonstrated that the formation of oxygen vacancies and the change of the Mn^{3+}/ Mn^{4+} ratio on the B-site play important roles to explain structural, magnetic and energetic properties of the substituted perovskite.

In $BiFeO_3$-$BiMnO_3$ system was already pointed out that, even though the Mn substitution does not alter the space group of $BiFeO_3$ for $x \leq 0.3$, the possible variation of the valence state of Mn manganese together the oxygen hiperstoistoichiometry as a function of temperature and oxygen pressure could affect the crystallographic properties, electrical conductivity and phase stability of $BiFe_{1-x}Mn_xO_{3+\delta}$ (Selbach, 2009, 2009). Excepting the communicated results on DSC investigation of $Bi_{1-x}La_xFe_{1-y}Mn_yO_3$ (x=0.1; y=0-0.5) (Tanasescu, 2010), no other work related to the thermodynamic behaviour of $Bi_{1-x}La_xFe_{1-y}Mn_yO_3$ were reported in the literature. In that study the evolution of heat of transformation and heat capacity in the temperature range of 573 – 1173 K was analyzed. The ferroelectric transition was shifted to a lower temperature for $Bi_{0.9}La_{0.1}FeO_3$ comparative to $BiFeO_3$, in agreement with literature data (Chen, 2008). However, a non-monotonous change of T_C, as well as of the thermochemical parameters is registered for the La and Mn co-doped compositions, depending on the Mn concentration, comparatively with undoped $BiFeO_3$. A sharp decline in the *T*c was pointed out for x=0.3. One reason to explain this behavior is sustained by the structural results which were already pointed out in the previous section. The increase of the manganese concentration determines the decrease of both *a* and *c* lattice parameters and therefore a gradual contraction of the unit cell volume. This evolution suggests that most of the manganese ions are more probably incorporated on the B-site as Mn^{4+}. Besides, as already was shown, in our samples the decreasing of the average grain size with the addition of both La and Mn solutes was observed in the case of presintered, as well as ceramics sintered at 1273 K (Ianculescu, 2009; Tanasescu, 2010). For finer particles where defect formation energies are likely to be reduced, the lattice defects, oxygen nonstoichiometry etc. appear to be sizable and significant changes in overall defect concentration are expected. So, an excess of Mn^{4+} ions and an increased oxygen nonstoichiometry are more likely. Due to the linear relationship between the Mn-O distortion and the Mn^{3+} content, one could expect to find in our samples a strong dependence of the energetic parameters on the Mn^{3+}/ Mn^{4+} ratio and the oxygen nonstoichiometry.

In order to understand how the thermodynamic properties are related to the oxygen and manganese content in the substituted $BiFeO_3$, the thermodynamic properties represented by the relative partial molar free energies, enthalpies and entropies of oxygen dissolution in the perovskite phase, as well as the equilibrium partial pressures of oxygen have been obtained in a large temperature range (923-1123 K) by using solid electrolyte electrochemical cells method.

The obtained results are plotted in Figures 18 - 20. At low temperatures, between 923 and ~950 K for x=0.3 and between 923 and ~1000 K for x=0.2, the $\Delta\overline{G}_{O_2}$ values are increasing with temperature (Fig. 18(a)). The same trend is accounted for the $\log p_{O_2}$ variation (Fig. 18(b)). The break points at ~963 K and ~993 K obtained for x=0.3 and x=0.2, respectively (Fig. 18 (a)) are consistent with the *T*c values of ferro-para transition in substituted samples. These values are near the ferroelectric Curie temperatures reported in the literature for $BiFe_{0.7}Mn_{0.3}O_3$ (926-957 K) and $BiFe_{0.8}Mn_{0.2}O_3$ (~990 K) with no La addition (Selbach, 2009; Sahu, 2007). However we have to notice that at the same Mn concentration x=0.3, the *T*c

value is slightly higher for the sample in which lanthanum is present, comparatively with the sample without La.

In Fig. 19 we represented the partial molar free energies of oxygen dissolution obtained in this study for $Bi_{0.9}La_{0.1}Fe_{0.8}Mn_{0.2}O_3$ and $Bi_{0.9}La_{0.1}Fe_{0.7}Mn_{0.3}O_3$ samples at temperatures lower than their specific ferroelectric transition temperatures, and for comparison, the $\Delta\overline{G}_{O_2}$ values of $BiFeO_3$. As one can see in Fig. 19, the partial molar free energies of oxygen dissolution in the substituted samples are highest than the $\Delta\overline{G}_{O_2}$ values obtained for $BiFeO_3$, suggesting the increasing oxygen vacancies concentration with doping. Determining the $\Delta\overline{H}_{O_2}$ and $\Delta\overline{S}_{O_2}$ values in particular temperature ranges until T_C in which the partial molar free energies are linear functions of temperature (Figs. 19 and 20) one can observe that for the substituted compounds, the $\Delta\overline{H}_{O_2}$ and $\Delta\overline{S}_{O_2}$ values strongly increase in the doped compounds. Due to the relative redox stability of the B^{3+} ions (at the same A-site composition), both the mobility and the concentration of the oxygen vacancies will be modified. However it was noticed that the increase in B-site substitution from x = 0.20 to x = 0.30 at temperatures below 1000 K is followed by the decrease of $\Delta\overline{H}_{O_2}$ and $\Delta\overline{S}_{O_2}$ values with ~117.6 kJ mol^{-1} and ~126 J mol^{-1} K^{-1} respectively (Fig. 20), suggesting the increase of the binding energy of oxygen and an increase of order in the oxygen sublattice of the perovskite-type structure with the Mn concentration.

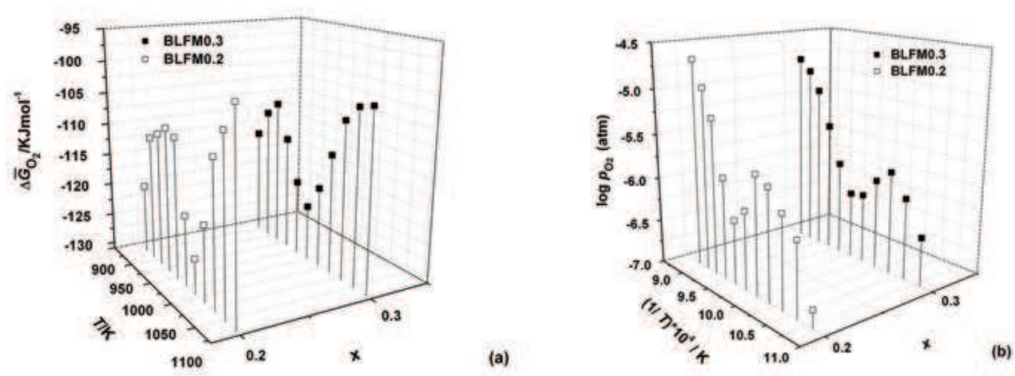

Fig. 18. Variation of $\Delta\overline{G}_{O_2}$ (a) and $\log p_{O_2}$ (b) with temperature and Mn content (x)

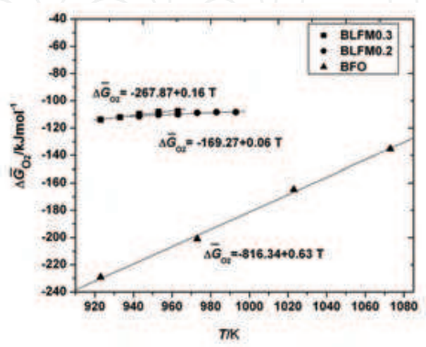

Fig. 19. Variation of $\Delta\overline{G}_{O_2}$ with temperature - linear fit in the temperature ranges under the ferroelectric transition temperatures

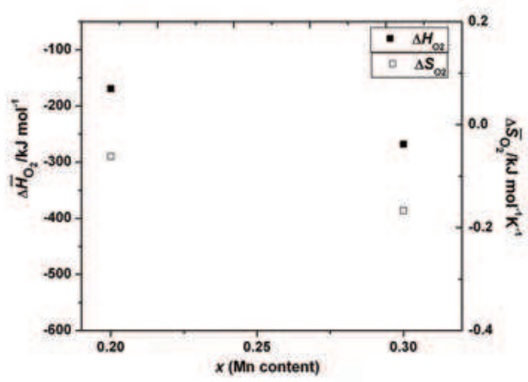

Fig. 20. $\Delta\overline{H}_{O_2}$ and $\Delta\overline{S}_{O_2}$ as a function of Mn content (x) at temperatures lower than T_C

After the ferroelectric transition temperatures and until 1043 K (for x=0.2), respectively until 1023 K (for x=0.3), a sharp decrease of the $\Delta\overline{G}_{O_2}$ values (Fig. 18(a)), together positive values of the enthalpies and entropies are revealed for both samples, indicating the decreasing of the thermodynamic driving force for oxygen vacancies formation and low ionic mobility. Taking into account the working conditions and the existing information as concerns the phase correlations of systems (Selbach, 2009, 2009, Carvalho, 2008), the dissociation reaction of the perovskite could be assumed to proceed in this temperature interval, $Bi_{0.9}La_{0.1}Fe_{1-x}Mn_xO_3$ being in equilibrium with other two solid phases, namely sillenite and mullite type-phases ($Bi_{25}Fe_{1-y}Mn_yO_{39}$ and $Bi_2Fe_{4-z}Mn_zO_9$, respectively). Increasing the temperature until 1083 K (for x=0.2) and 1073 K (for x=0.3), the equilibrium will be driven back to the perovskite formation, the $\Delta\overline{G}_{O_2}$ values of the sample with x=0.3 keeping higher than those of the sample with x=0.2 (Fig. 18(a)). At 1083 K (for x=0.2) and 1073 K (for x=0.3), the registered $\Delta\overline{G}_{O_2}$ values have practically the same values as for the samples before decomposition. The next phase transition registered at 1093 K for $Bi_{0.9}La_{0.1}Fe_{0.7}Mn_{0.3}O_3$ is qualitatively in concordance with the transition to the γ polymorph which was previously identified in the literature for $BiFeO_3$ at 1198-1203K (Arnold, 2010; Palai, 2008; Selbach, 2009) and for $BiFe_{0.7}Mn_{0.3}O_3$ at 1145-1169 (Selbach, 2009). The temperature of transition to the γ phase corresponding to $Bi_{0.9}La_{0.1}Fe_{0.8}Mn_{0.2}O_3$ could be higher than 1123 K; it was not registered in our present experiment because the highest temperature of these measurements was 1123 K.

The obtained results evidenced the complex behavior of the partial molar thermodynamic data in substituted samples, suggesting a change of the predominant defects concentration as a function of temperature range and Mn concentration. Increasing the manganese content, the decreasing of the ferroelectric Curie temperature and of the transition temperature from paraelectric to γ phase it is noted.

To further evaluate the previous results, the influence of the oxygen stoichiometry change on the thermodynamic properties has been investigated. The variation of the partial molar thermodynamic data of $Bi_{0.9}La_{0.1}Fe_{0.8}Mn_{0.2}O_3$ (noted as BLFM0.2) and $Bi_{0.9}La_{0.1}Fe_{0.7}Mn_{0.3}O_3$ (noted as BLFM0.3) was examined before and after two successive titrations by the same relative oxygen stoichiometry change of $\Delta\delta$ = 0.02 in the oxygen excess region (Figures 21 and 22). Thus, the effect of the oxygen stoichiometry can be correlated with the influence of the substituent.

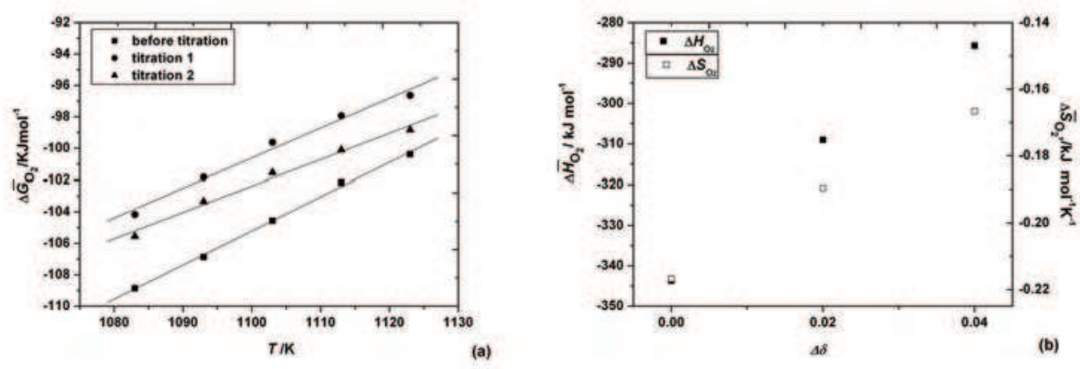

Fig. 21. (a) Variation of $\Delta\overline{G}_{O_2}$ with temperature and oxygen stoichiometry change for $Bi_{0.9}La_{0.1}Fe_{0.8}Mn_{0.2}O_{3+\delta}$; (b) $\Delta\overline{H}_{O_2}$ and $\Delta\overline{S}_{O_2}$ of $Bi_{0.9}La_{0.1}Fe_{0.8}Mn_{0.2}O_{3+\delta}$ as a function of the oxygen stoichiometry change ($\Delta\delta$ = 0; 0.02; 0.04)

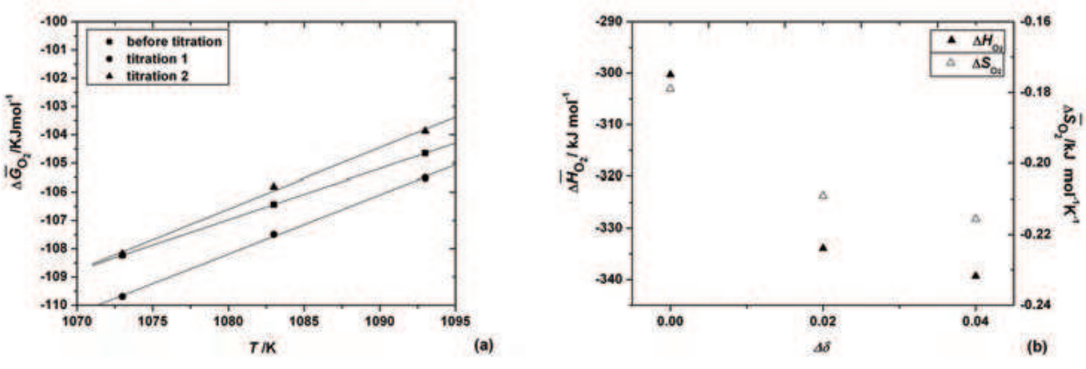

Fig. 22. (a) Variation of $\Delta\overline{G}_{O_2}$ with temperature and oxygen stoichiometry change for $Bi_{0.9}La_{0.1}Fe_{0.7}Mn_{0.3}O_{3+\delta}$; (b) $\Delta\overline{H}_{O_2}$ and $\Delta\overline{S}_{O_2}$ of $Bi_{0.9}La_{0.1}Fe_{0.7}Mn_{0.3}O_{3+\delta}$ as a function of the oxygen stoichiometry change ($\Delta\delta$ = 0; 0.02; 0.04)

For x=0.2 higher values of the partial molar thermodynamic data are obtained after titration (Fig. 21). It is expected that the change in $\Delta\overline{S}_{O_2}$ with δ in this case to be essentially determined by the change in S_O (config) and, therefore, the oxygen randomly distribute on the oxygen sites. Instead for x=0.3, both the variations of enthalpy and entropy decrease with the stoichiometry change (Fig. 22(b)), suggesting the increase in the binding energy of oxygen and change of order in the oxygen sublattice of the perovskite-type structure comparatively with the undoped compound. However it is interesting to note that the enthalpies obtained for x=0.3 after the first and the second titrations are near each other, suggesting a smaller dependence of the $\Delta\overline{H}_{O_2}$ on the oxygen stoichiometry change at higher departure from stoichiometry. This result tends to agree with the assumption that metal vacancies prevail, since a value for enthalpy which is independent of nonstoichiometry is expected for randomly distributed and noninteracting metal vacancies (van Roosmalen, 1994; Tanasescu, 2005). The model based on excess oxygen compensated by cation vacancies and partial charge disproportionation of manganese ions was also proposed for other related systems, like $LaMnO_{3+\delta}$ (van Rosmallen, 1995; Töpfer, 1997),

$BiMnO_{3+\delta}$ (Sundaresan, 2008), $BiFe_{0.7}Mn_{0.3}O_{3+\delta}$ (Selbach, 2009), $La_{0.5}Bi_{0.5}Mn_{0.5}Fe_{0.5}O_{3+\delta}$ (Kundu, 2008). However, the model could not explain the observed relationship in the entire oxygen-excess region. This statement was also discussed in the case of $LaMnO_{3+\delta}$ (Mizusaki, 2000; Nowotny, 1999; Tanasescu 2005) and could be subject for further discussion.

Considering the partial pressure of oxygen as a key parameter for the thermodynamic characterization of the materials, we investigated the variation of $\log p_{O_2}$ with the temperature, oxygen stoichiometry and the concentration of the B-site dopant (Fig. 23). Before titration, the $\log p_{O_2}$ values of the $Bi_{0.9}La_{0.1}Fe_{0.7}Mn_{0.3}O_3$ are higher than $\log p_{O_2}$ for $Bi_{0.9}La_{0.1}Fe_{0.8}Mn_{0.2}O_3$, excepting the value at 1123 K which is smaller for x=0.3 comparatively with the corresponding value for x=0.2, the result being correlated with the structural phase transformation noted for the composition with x=0.3 under 1123 K.

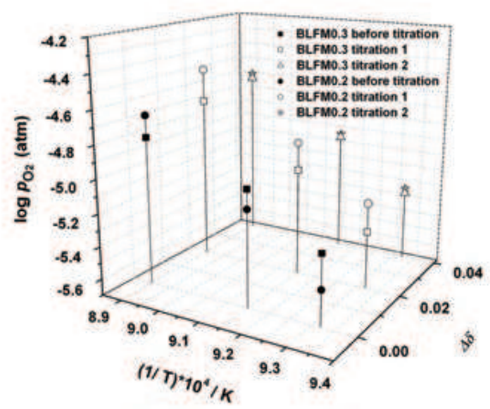

Fig. 23. Variation of $\log p_{O_2}$ with temperature and oxygen stoichiometry change

It is obtained that for both compounds, after titration, at the same deviation of the oxygen stoichiometry, $\log p_{O_2}$ shifted to higher values with increasing temperature. At the same temperature, the high deviation in the $\log p_{O_2}$ values with the stoichiometry change is obtained for the sample with x=0.2. Besides, at x=0.2, higher values of $\log p_{O_2}$ are obtained after the second titration, even though, increasing deviation from stoichiometry, a smaller increase of the partial pressure of oxygen was noted (Fig. 23). This could be explained by the fact that at high temperature, less excess oxygen is allowed. The sample with x=0.3 presents a smaller dependence of the $\log p_{O_2}$ on the oxygen nonstoichiometry. For small deviation from stoichiometry ($\Delta\delta$=0.02), a small decrease in $\log p_{O_2}$ values is obtained, but after the second titration, the partial pressure increase again. At 1073 K, after the second titration, the same value as before titration is obtained. Increasing temperature to 1123 K, $\log p_{O_2}$ values increase again comparatively with the value before titration.

The obtained results could be correlated with some previously reported conductivity measurements. Singh et al (Singh, 2007) reported that small manganese doping in thin films of $BiFeO_3$ improved leakage current characteristic in the high electric field region, reducing the conductivity; others authors noted the increasing of the conductivity with increasing manganese content (Chung, 2006; Selbach, 2009, 2010). If the polaron hopping mechanism is supposed for the electrical conductivity at elevated temperatures, the electronic conductivity will increase in the samples with hiperstoichiometry. According to the evolution of the

partial molar thermodynamic data of the oxygen dissolution, a decrease in the oxygen ionic conductivity (together the increasing of the electronic conductivity due to the electron-hole concentration increasing) will result in the sample with increased Mn content.
Even though there are disagreements between different works regarding the nature and the symmetry of the high temperature phases in the pure and substituted $BiFeO_3$, based on our data, we would like to point out that, in the condition of our experimental work, we may close to the stability limit of the Mn doped materials at temperatures around 1123 K. This is in accordance with theoretical consideration of the stability of ABO_3 compounds based on Goldschmidt tolerance factor relationship (Goldschmidt, 1926). The evolution with temperature and oxygen stoichiometry of the thermodynamic data suggest that excess oxygen causing an increase of the tolerance factor of the system will lead to the stabilization of the cubic phase at lower temperature with increasing the departure from stoichiometry.
At this point further studies are in progress, so that correlations could be established with the observed properties at different departures of oxygen stoichiometry, in both deficit and excess region for $Bi_{0.9}La_{0.1}Fe_{1-x}Mn_xO_3$ materials.

4. Conclusions

$Bi_{1-x}Ba_xFe_{1-x}Ti_xO_3$ ($0 \le x \le 0.30$) and $Bi_{0.9}La_{0.1}Fe_{1-x}Mn_xO_3$ ($0 \le x \le 0.50$) ceramics were prepared by the conventional mixed oxides route, involving a two-step sintering process. Single phase perovskite compositions resulted for all the investigated ceramics, in the limit of XRD accuracy. For both cases, the presence of foreign cations replacing Bi^{3+} and/or Fe^{3+} in the perovskite lattice induces the diminishing of the rhombohedral distortion and causes significant microstructural changes, mainly revealed by the obvious decrease of the average grain size.
In order to evidence how the appropriate substitutions could influence the stability of the perovskite phases and then to correlate this effect with the charge compensation mechanism, the thermodynamic data represented by the relative partial molar free energies, enthalpies and entropies of the oxygen dissolution in the perovskite phase, as well as the equilibrium partial pressures of oxygen have been obtained by solid state electrochemical (EMF) method. The influence of the oxygen stoichiometry change on the thermodynamic properties was examined using the data obtained by a coulometric titration technique coupled with EMF measurements.
New features related to the thermodynamic stability of the multiferroic $Bi_{1-x}Ba_xFe_{1-x}Ti_xO_3$ and $Bi_{0.9}La_{0.1}Fe_{1-x}Mn_xO_3$ ceramics were evidenced, the thermodynamic behavior being explained not only by the structural changes upon doping, but also by the fact that the energetic parameters are extremely sensitive to the chemical defects in oxygen sites.
The decreasing of the ferroelectric – paraelectric transition temperature in the substituted samples was evidenced by both EMF and DSC measurements. Besides, the phase transition qualitatively corresponding to the phase transformation from paraelectric to a new high temperature phase was evidenced and the partial molar thermodynamic data describing the different phase stability domains were presented for the first time.
Bearing in mind the role of charge ordering and of the defects chemistry in explaining the electrical, magnetic and thermodynamic behavior of the doped perovskite-type oxides, it should be possible to find new routes for modifying the properties of these materials by controlling the average valence in B-site and the oxygen nonstoichiometry. Preparation

method also strongly could influence the behavior of the powder in terms of non-stoichiometry, which ultimately will affect its electrical properties since they are dependent upon the presence of oxygen ion vacancies in the lattice. Besides the doping with various foreign cations, the decreasing of the grain sizes, as well as the thin film technology could be efficient methods for tuning the electrical, magnetic and thermodynamic properties of $BiFeO_3$-based compounds to be used as multiferroic materials.

5. Acknowledgments

Support of the EU (ERDF) and Romanian Government that allowed for acquisition of the research infrastructure under POS-CCE O 2.2.1 project INFRANANOCHEM - Nr. 19/01.03.2009, is gratefully acknowledged. This work also benefits from the support of the PNII-IDEAS program (Project nr. 50 / 2007).

6. References

Arnold, D. C.; Knight, K. S.; Catalan, G.; Redfern, S. A. T.; Scott, J. F.; Lightfoot, P. & Morrison, F. D. (2010). The β-to-γ transition in $BiFeO_3$: a powder neutron diffraction study. *Advanced Functional Materials,* Vol. 20, No. 13, pp. 2116-2123, ISSN 1616-301X

Azuma, M.; Kanda, H.; Belik, A. A.; Shimakawa, Y. & Takano, M. (2007). Magnetic and structural properties of $BiFe_{1-x}Mn_xO_3$, *Journal of Magnetism and Magnetic Materials*, Vol. 310, No. 2, Part. 2, pp. 1177 -1179, ISSN 0304-8853

Bogatko, V. V.; Fadeeva, N. V.; Gagulin, V. V.; Korchagina, S. K. & Shevchuk, Y. A. (1998). Structure and properties of $BiFeO_3$-$LaMnO_3$ seignettomagnetic solid-solutions, *Inorganic Materials*, Vol. 34, No. 11, pp. 1141-1143, ISSN 0020-1685

Boyd, G. R.; Kumar, P. & Phillpot, S. R. (2011). Multiferroic thermodynamics, *Materials Science,* arXiv:1101.5403v1

Buscaglia, M. T.; Mitoseriu, L.; Buscaglia, V.; Pallecchi, I.; Viviani, M.; Nanni, P. & Siri, A. S. (2006). Preparation and characterization of the magneto-electric $xBiFeO_3$–$(1−x)BaTiO_3$ ceramics, *J. Eur. Ceram. Soc.*, Vol. 26, No. 14, pp. 3027-3030, ISSN 0955-2219

Carvalho, T. T. & Tavares, P. B. (2008). Synthesis and thermodynamic stability of multiferroic $BiFeO_3$, *Materials Letters*, Vol. 62, No. 24, pp. 3984-3986, ISSN. 0167-577X

Catalan, G. & Scott, J. F. (2009). Physics and application of bismuth ferrite. *Advanced Materials*, Vol. 21, No. 14, pp. 2463-2485, ISSN: 09359648

Charette, G. G. & Flengas, S. N. (1968). Thermodynamic Properties of the Oxides of Fe, Ni, Pb, Cu, and Mn, by EMF Measurements, *J. Electrochem. Soc.,* Vol. 115, No. 8, pp. 796-804

Chen, J. R.; Wang, W. L.; Li, J.-B. & Rao, G. H. (2008). X-ray diffraction analysis and specific heat capacity of $(Bi_{1-x}La_x)FeO_3$ perovskites, *J. Alloys Compd.*, Vol. 459, No. 1-2, pp. 66-70, ISSN 0925-8388

Chung, C. F.; Lin, J. P.; & Wu, J. M. (2006). Influence of Mn and Nb dopants on electric properties of chemical-solution-deposited $BiFeO_3$ films, *Appl. Phys. Lett.*, Vol. 88, No. 24, pp. 242909.1-242909.3, ISSN 0003-6951

Ederer, C. & Spaldin, N. A. (2005). Weak ferromagnetism and magnetoelectric coupling in bismuth ferrite, *Phys. Rev.*, Vol. B 71, No. 6, pp. 060401.1 - 060401.4

Ederer, C. & Spaldin, N. A. (2005). Influence of strain and oxygen vacancies on the magnetoelectric properties of multiferroic bismuth ferrite, *Physical Review*, Vol. 71, No. 22, pp. 224103.1-224103.9

Fukumura, H.; Matsui, S.; Tonari, N.; Nakamura, T.; Hasuike, N.; Nishio, K.; Isshiki, T. & Harima, H. (2009). Synthesis and characterization of Mn-doped $BiFeO_3$ nanoparticles, *Acta Phisica Polonica A*, Vol. 116, No.1, pp. 47-50

Gagulin, V. V.; Korchagina, S. K. ; Shevchuk, Y. A. ; Fadeeva, N. V. & Bogatko, V. V. (1997). Synthesis and physical properties of new high temperature seignettomagnetics in the systems with perovskite type structure, *Ferroelectrics*, Vol. 204, No. 1, pp. 345-355

Goldschmidt, V. M. (1926). The laws of crystal chemistry, *Naturwissenschaften*, Vol. 14, pp. 477-485

Gu, Y. H.; Wang, Y.; Chen, F.; Chan, H. L. W. & Chen, W. P. (2010). Nonstoichiometric $BiFe_{0.9}Ti_{0.05}O_3$ multiferroic ceramics with ultrahigh electrical resistivity, *Journal of Applied Physics*, Vol. 108, No. 9, pp. 094112.1 -094112.5

Habouti, S.; Solterbeck, C.H. & Es-Souni, M.; (2007). $LaMnO_3$ effects on the ferroelectric and magnetic properties of chemical solution deposited $BiFeO_3$ thin films, *Journal of Applied Physics*, Vol. 102, No. 7, pp. 074107.1-074107.4, ISSN 0021-8979

Ianculescu, A.; Mitoseriu, L.; Chiriac, H.; Carnasciali, M. M.; Braileanu, A. & Trusca, R. (2008). Preparation and magnetic properties of the $(1-x)BiFeO_3 - xBaTiO_3$ solid solutions, *J. Optoel. & Adv. Mater.*, Vol. 10, No. 7, pp. 1805-1809, ISSN 1454-4164

Ianculescu, A.; Prihor, F.; Postolache, P.; Mitoseriu, L.; Dragan, N. & Crisan, D. (2009). Preparation and properties of Mn-doped $La_{0.1}Bi_{0.9}FeO_3$ ceramics, *Ferroelectrics,* Vol. 391, No. 1, pp. 67-75

Ismailzade, I. H.; Ismailov, R. M.; Alekberov, A. I. & Salaev F. M. (1981). Investigation of the magnetoelectric effect in the system $BiFeO_3$–$LaFeO_3$, Physica Status Solidi (a), Vol. 66, No. 1, pp. 119–123

Ivanova, V. V.; Gagulin, V. V.; Korchagina, S. K.; Shevchuk, Y. A. & Bogatko V. V. (2003). Synthesis and properties of $BiFeO_3$–$DyMnO_3$ solid solutions, *Inorganic Materials*, Vol. 39, No. 7, pp. 745-748, ISSN 0020-1685

Jiang, Q. H.; Nan C. W. & Shen, Z. J. (2006). Synthesis and Properties of Multiferroic La-Modified $BiFeO_3$ Ceramics, *J. Am. Ceram. Soc*., Vol. 89, No. 7, pp. 2123-2127

Jonker, G. H. & van Santen, J. H. (1953). Magnetic compounds with perovskite structure, *Physica*, Vol. 19, No. 1-12, pp. 120-130

Kelley, K. K. (1960).*U. S. Bur of Mines Bull*, Vol. 584

Kelley, K. K. & King, E. G.; (1961) *U. S. Bur of Mines Bull*., Vol. 592

Kim, S. J. & Cheon, C. II. (2004). Weak ferromagnetism in the ferroelectric $BiFeO_3$- $ReFeO_3$-$BaTiO_3$ solid solution (Re=Dy, La). *Journal of Applied Physics*, Vol. 96, No.1, pp. 468-474

Kim, S. J.; Cheon, C. I.; Kang, H. J. & Jang, P. W. (2007). High temperature properties of multiferroic $BiFeO_3$-$DyFeO_3$-$BaTiO_3$ solid solutions, *Journal of the European Ceramic Society*, Vol. 27, No. 13-15, pp. 3951-3954, ISSN 0955-2219

Kothari, D.; Reddy, V. R.; Gupta, A.; Phase, D. M.; Lakshmi, N.; Deshpande, S. K. & Awasthi, A. M. (2007). Study of the effect of Mn doping on the $BiFeO_3$ system, *Journal of Physics: Condensed Matter,* Vol.19, No. 13, pp. 136202.1-136202.8

Kumar, M. M.; Srinivas, A.;. Kumar, G. S. & Suryanarayana, S. V. (1999). Investigation of the magnetoelectric effect in $BiFeO_3$-$BaTiO_3$ solid solutions, *J. Phys.: Condens. Matter,* Vol. 11, No. 41, 8131

Kumar, M. M.; Srinivas, A. & Suryanarayana, S. V. (2000). Structure property relations in $BiFeO_3$/ $BaTiO_3$ solid solutions, *Journal of Applied Physics*, Vol. 87, No. 2, pp. 855-862

Kumar, M. M.; Palkar, V. R.; Srinivas, K. & Suryanarayana, S. V. (2000). Ferroelectricity in a pure $BiFeO_3$ ceramic, *Appl. Phys. Lett*., Vol. 76, No. 19, pp. 2764-2766

Kundu, A. K.; Ranjith, R.; Kundys, B.; Nguyen, N.; Caignaert, V.; Pralong, V.; Prellier, W. & Raveau, B. (2008). A multiferroic ceramic with perovskite structure : $(La_{0.5}Bi_{0.5})(Mn_{0.5}Fe_{0.5})O_{3.09}$, *Applied Physics Letters*, Vol. 93, No. 5, pp. 052906.1-052906.3, ISSN 0003-6951

Maignan, A.; Martin, C. & Raveau, B. (2000). Magnetoresistance properties in manganese and cobalt oxides, *Journal of Superconductivity,* Vol. 13, No. 2, pp. 313-328

Marinescu, C.; Sofronia, A. & Tanasescu, S. (in press). Differential scanning calorimetry: Part A: temperature calibration of differential scanning calorimeter (DSC) in the heating mode, *Revue Roumaine de Chimie*, RRC 251

Mitoseriu, L. (2005). Magnetoelectric phenomena in single-phase and composite systems, *Boletin de la Sociedad Espanola de Ceramica y Vidrio*. Vol. 44, No. 3, pp. 177-184

Mizusaki, J.; Mori, N.; Takai, H.; Yonemura, Y.; Minamiue, H.; Tagawa, H.; Dokiya, M.; Inaba, H.; Naraya, K.; Sasamoto T. & Hashimoto, T. (2000). Oxygen nonstoichiometry and defect equilibrium in the perovskite-type oxides $La_{1-x}Sr_xMnO_{3+d}$, *Solid State Ionics*, Vol. 129, No. 1-4, pp. 163-177, ISSN 0167-2738

Nowotni, J. & Rekas, M. (1998). Defect chemistry of (La,Sr)MnO_3, *Journal of the American Ceramic Society*, Vol. 81, No. 1, pp. 67-80

Palai, R.; Katiyar, R. S.; Schmid, H.; Tissot, P.; Clark, S. J.; Robertson, J.; Redfern, S. A. T.; Catalan, G. & Scott, J. F. (2008). β phase and γ-β metal-insulator transition in multiferroic $BiFeO_3$, *Physical Review*, Vol. B 77, No. 1, pp. 014110.1-014110.11

Palkar, V. R. & Pinto, R. (2002). $BiFeO_3$ thin films: Novel effects, *Pramana Journal of Physics*, Vol. 58, No. 5-6, pp.1003-1008

Palkar, V. R.; Darshan, C.; Kundaliya, C. & Malik, S. K. (2003). Effect of Mn substitution on magnetoelectric properties of bismuth ferrite system, *J. Appl. Phys*., Vol. 93, No. 7, pp. 4337-4339, ISSN 0021-8979

Pradhan, D. K.; Choudhary, R. N. P.; Tirado, C. M. & Katiyar, R. S. (2008). Effect of La/Mn substitution on electrical properties of $BiFeO_3$ multiferroics, *Indian Journal of Engineering & Materials Sciences*, Vol. 15, pp. 87-90, ISSN 0971-4588

Prihor, F.; Postolache, P.; Curecheriu, L.; Ianculescu, A. & Mitoseriu, L. (2009). Functional properties of the (1- x) $BiFeO_3$ – $xBaTiO_3$ solid solutions, *Ferroelectrics*, Vol. 391, No.1, pp. 76-82, ISSN 0015-0193

Prihor Gheorghiu, F.; Ianculescu, A.; Postolachea, P.; Lupu, N.; Dobromira, M.; Luca, D. & Mitoseriu, L. (2010). Preparation and properties of $(1-x)BiFeO_3$ – $xBaTiO_3$ multiferroic ceramics, *J. Alloy Compd*., Vol. 506, No. 2, pp. 862-867

Qi, X.; Dho, J. & Tomov, R. (2005). Greatly reduced leakage current and conduction mechanism in aliovalent-ion-doped $BiFeO_3$, *Applied Physics Letters*, Vol. 86, No. 6, pp. 062903.1-062903.3

Ramesh, R. & Spaldin, N. A. (2007). Multiferroics: progress and prospects in thin films, *Nature Publishing Group*, Vol. 6, No.1, pp. 21-29

Sahu, J. R. & Rao, C. N. R. (2007). Beneficial modification of the properties of multiferroic $BiFeO_3$ by cation substitution, *Solid State Sci*., Vol. 9, No. 10, pp. 950-954

Selbach, S. M.; Tybell, T.; Einarsrud, M.-A. & Grande, T. (2009). Structure and properties of multiferroic oxygen hyperstoichiometric $BiFe_{1-x}Mn_xO_{3+\delta}$. *Chemistry of Materials*, Vol. 21, No. 21, pp. 5176-5186

Selbach, S. M.; Tybell, T.; Einarsrud, M.-A. & Grande, T. (2009). High-temperature semiconducting cubic phase of $BiFe_{0.7}Mn_{0.3}O_{3+\delta}$, *Physical Review*, Vol. 79, No. 21, pp. 214113.1-214113.5

Selbach, S. M.; Tybell, T.; Einarsrud, M.-A. & Grande, T. (2010). Phase transitions, electrical conductivity and chemical stability of $BiFeO_3$ at high temperatures. *Journal of Solid State Chemistry*, Vol. 183, No. 5, pp. 1205-1208

Singh, S. K. & Ishiwara, H. (2007). Microstructure and frequency dependent electrical properties of Mn-substituted $BiFeO_3$ thin films. *Journal of Applied Physics*, Vol. 102, No. 9, pp. 094109.1-094109.5, ISSN 0021-8979

Singh, A.; Pandey, V.; Kotnala, R. K. & Pandey, D. (2008). Direct evidence for multiferroic magnetoelectric coupling in 0.9 $BiFeO_3$-0.1 $BaTiO_3$, *Phis. Rev.Lett.*, Vol. 101, 247602

Singh, A.; Patel, J. P. & Pandey, D. (2009). High temperature ferroic phase transition and evidence of paraelectric cubic phase in the multiferroic 0.8 $BiFeO_3$-0.2 $BaTiO_3$. *Applied Physics Letters*, Vol. 95, No. 14, pp. 142909.1-142909.3

Stroppa, A. & Picozzi, S. (2010). Hybrid functional study of proper and improper multiferroics, *Physical Chemistry Chemical Physics*, Vol. 12, No. 20, pp. 5405-5416

Sundaresan, A.; Mangalam, R. V. K.; Iyo, A.; Tanaka, Y. & Rao, C. N. R. (2008). Crucial role of oxygen stoichiometry in determining the structure and properties of $BiMnO_3$, *J. Mater. Chem.*, Vol. 18, pp. 2191-2193

Takahashi, K. & Tonouchi, M. (2007). Influence of manganese doping in multiferroic bismuth ferrite thin films, *Journal of Magnetism and Magnetic Materials*, Vol. 310, No. 2, pp. 1174-1176, ISSN 0304-8853

Tanasescu, S.; Maxim, F.; Teodorescu, F. & Giurgiu, L. (2008). The influence of composition and particle size on spin dynamics and thermodynamic properties of some magnetoresistive perovskites, *Journal of Nanoscience and Nanotechnology*, Vol. 8, pp. 914–923

Tanasescu, S.; Grecu, M. N.; Marinescu, C.; Giurgiu, L. M.; Chiriac, H. & Urse, M. (2009). Effects of dopants and oxygen nonstoichiometry on the thermodynamic, magnetic and electrical properties of micro- and nanostructured perovskite-type materials, *Advances in Applied Ceramics*, Vol. 108, No. 5, pp. 273-279

Tanasescu, S.; Marinescu, C.; Sofronia, A.; Ianculescu, A. & Mitoseriu, L. (2010), Communication at *Electroceramics XII,* 13th - 16th of June 2010, Trondheim, Norway

Tanasescu, S.; Marinescu, C.; Maxim, F.; Sofronia, A. & Totir, N. (2011). Evaluation of manganese and oxygen content in $La_{0.7}Sr_{0.3}MnO_{3-\delta}$ and correlation with the thermodynamic data, *Journal Solid State Electrochemistry*, Vol. 15, No. 1, pp. 189-196

Töfield, B. C. & Scott, W. R. (1974). Oxidative nonstoichiometry in perovskites, an experimental survey; the defect structure of an oxidized lanthanum manganite by powder neutron diffraction, *J. Solid State Chem.,* Vol. 10, No. 3, pp. 183-194

Töpfer, J. & Goodenough, J. B. (1997). Transport and magnetic properties of the perovskites $La_{1-y}MnO_3$ and $LaMn_{1-z}O_3$, *Chem. Mater.*, Vol. 9, No. 6, pp. 1467–1474

van Roosmalen, J. A. M. & Cordfunke, E. H. P. (1994). The defect chemistry of $LaMnO_{3+\delta}$: 5. Thermodinamics, *Journal of Solid State Chemistry*, Vol. 110, No. 1, pp. 113-117

van Roosmalen, J. A. M.; van Vlaanderen, P.; Cordfunke, *E. H. P.;* Ijdo, W. L. & Ijdo, D. J. W. (1995). Phases in the perovskite-type $LaMnO_{3d}$ solid solution and the La_2O_3–Mn_2O_3 phase diagram, *J. Solid State Chem*., Vol. 114, pp. 516–23

Wang, Y. P.; Zhou, L.; Zhang, M. F.; Chen, X. Y.; Liu, J. M. & Liu, Z. G. (2004). Room temperature saturated ferroelectric polarization in $BiFeO_3$ ceramics synthesized by rapid liquid phase sintering, *Applied Physics Letters*, Vol. 84, No. 10, id. 1731

Wang, N.; Cheng, J.; Pyatakov, A.; Zvezdin, A. K.; Li, J. F.; Cross, L. E. & Viehland, D. (2005). Multiferroic properties of modified $BiFeO_3$-$PbTiO_3$-based ceramics: Random-field induced release of latent magnetization and polarization, *Phys. Rev*., Vol. B 72, No. 10, pp. 390-392, ISSN 1099-4734

Wang, H.; Huang, H. & Wang, B. (2010). Effect of Mn substitution for Fe in multiferroic $BiFeO_3$: a first-principles study, *Science of Advanced Materials,* Vol. 2, No. 2, pp. 184-189

Warren, W. L.; Vanheusden, K.; Dimos, D.; Pike, G. E. & Tuttle, B. A. (1996), Oxygen vacancy motion in perovskite oxides, *Journal of the American Ceramic Society*, Vol. 79, No. 2, pp. 536–538

Yuan, G. L.; Or, S. W.; Wang, Y. P.; Liu, Z. G. & Liu, J. M. (2006). Preparation and multi-properties of insulated single-phase $BiFeO_3$ ceramics, *Solid State Communication*, Vol. 138, No. 2, pp. 76-81

Zheng, X.; Xu, Q.; Wen, Z.; Lang, X.; Wu, D.; Qiu, T. & Xu, M. X. (2010). The magnetic properties of La doped and codoped $BiFeO_3$, *Journal of Alloys and Compounds*, Vol. 499, No.1, pp. 108-112

Zhu, W. M. & Ye, Z. G. (2004). Effects of chemical modification on the electrical properties of $0.67BiFeO_3$−$0.33PbTiO_3$ ferroelectric ceramics, *Ceram. Int*., Vol. 30, No. 7, pp. 1435-1442

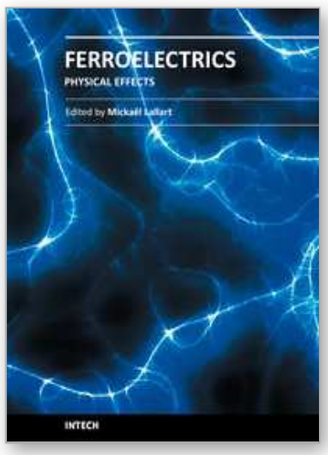

Ferroelectrics - Physical Effects

Edited by Dr. MickaÃ«l Lallart

ISBN 978-953-307-453-5
Hard cover, 654 pages
Publisher InTech
Published online 23, August, 2011
Published in print edition August, 2011

Ferroelectric materials have been and still are widely used in many applications, that have moved from sonar towards breakthrough technologies such as memories or optical devices. This book is a part of a four volume collection (covering material aspects, physical effects, characterization and modeling, and applications) and focuses on the underlying mechanisms of ferroelectric materials, including general ferroelectric effect, piezoelectricity, optical properties, and multiferroic and magnetoelectric devices. The aim of this book is to provide an up-to-date review of recent scientific findings and recent advances in the field of ferroelectric systems, allowing a deep understanding of the physical aspect of ferroelectricity.

InTech Europe
University Campus STeP Ri
Slavka Krautzeka 83/A
51000 Rijeka, Croatia
Phone: +385 (51) 770 447
Fax: +385 (51) 686 166
www.intechopen.com

InTech China
Unit 405, Office Block, Hotel Equatorial Shanghai
No.65, Yan An Road (West), Shanghai, 200040, China
中国上海市延安西路65号上海国际贵都大饭店办公楼405单元
Phone: +86-21-62489820
Fax: +86-21-62489821

IntechOpen